NANO LETTERS

pubs.acs.org/NanoLett Letter

Thermoelectric Enhancement in Single Organic Radical Molecules

Juan Hurtado-Gallego,[○] Sara Sangtarash,[○] Ross Davidson,*[,○] Laura Rincón-García, Abdalghani Daaoub, Gabino Rubio-Bollinger, Colin J. Lambert, Vasily S. Oganesyan, Martin R. Bryce,* Nicolás Agraït,* and Hatef Sadeghi*

Cite This: *Nano Lett.* 2022, 22, 948−953 Read Online

ACCESS | Metrics & More | Article Recommendations | Supporting Information

ABSTRACT: Organic thermoelectric materials have potential for wearable heating, cooling, and energy generation devices at room temperature. For this to be technologically viable, high-conductance (G) and high-Seebeck-coefficient (S) materials are needed. For most semiconductors, the increase in S is accompanied by a decrease in G. Here, using a combined experimental and theoretical investigation, we demonstrate that a simultaneous enhancement of S and G can be achieved in single organic radical molecules, thanks to their intrinsic spin state. A counterintuitive quantum interference (QI) effect is also observed in stable Blatter radical molecules, where constructive QI occurs for a *meta*-connected radical, leading to further enhancement of thermoelectric properties. Compared to an analogous closed-shell molecule, the power factor is enhanced by more than 1 order of magnitude in radicals. These results open a new avenue for the development of organic thermoelectric materials operating at room temperature.

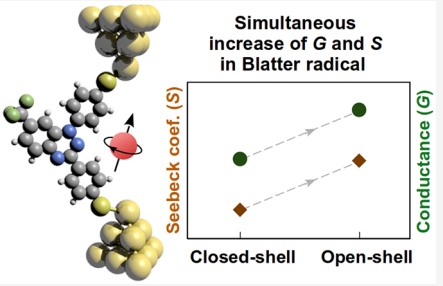

KEYWORDS: *Energy harvesting, organic thermoelectricity, single radical molecules, quantum transport*

Thermoelectric (TE) materials enable the direct conversion of thermal energy to electricity and are expected to play a key role in future energy-saving technologies.[1−3] TE devices can function as power generators through the Seebeck effect, or as solid-state coolers through the Peltier effect. Inorganic materials have been extensively studied for thermoelectricity. However, not only is their thermoelectric efficiency insufficient to meet the requirements of current energy needs, but they are also toxic, are difficult to process, and have limited global supply. In this regard, the ability to control and optimize electrical, thermal, and thermoelectric transport in other materials is a crucial stepping stone in the design, development, and operation of energy conversion technologies.[3−5] To enhance the efficiency of thermoelectric materials, their electrical conductance (G) and Seebeck coefficient (S) should be increased simultaneously.[6−8] For most semiconductors,[9,10] the increase in S is accompanied by a decrease in G, which leads to a low power factor (GS^2).[11] For example, the thermoelectric efficiency of organic polymers is limited by their low G or high thermal conductance, although several organic polymers achieve values of S in the range of 0.1−1 mV/K.[12−16]

In contrast, sharp transport features due to electron transport through molecular frontier orbitals in single organic molecules make them very attractive for enhancing G and S, simultaneously.[17] Single organic molecules also facilitate bottom-up functionalization and atomically precise engineering of their properties that are not accessible in other materials. Despite over a decade of development, the value for S in single organic molecules at room temperature is usually below ±20 μV/K.[1−3] This is because the frontier orbitals of most molecules are far from the Fermi energy (E_F) of the electrodes. If the energies of the frontier orbitals where transport resonances occur are moved close to E_F, simultaneous enhancement of G and S is expected. This is a consequence of G being proportional to the electron transmission function $T(E)$, while S is proportional to its slope via the relation[18]

$$G = G_0 T(E_F), \quad S = S_0 \frac{\mathrm{d}\ln(T(E))}{\mathrm{d}E}\bigg|_{E=E_F} \tag{1}$$

where $G_0 = 7.74 \times 10^{-5}$ (Ω^{-1}) is the conductance quantum and $S_0 = -2.44 \times 10^{-8} T$ (WΩ/K), where T is the temperature. For this reason, molecules with radical features, such as partially filled orbitals, can be very attractive. This is because the partially filled orbital (spin orbital) has a tendency to gain or lose an electron and move its energy level close to the Fermi energy E_F of the electrodes.[17]

With this in mind, we have designed and synthesized the 1,2,4-benzotriazin-4-yl (Blatter) radical molecules **1** and **2**, which are air-stable, neutral radicals that can be modified in a modular fashion and form a single-molecule junction,[19] and the closed-shell (non-radical) quinazoline analogue **3** with

Received: September 24, 2021
Revised: December 7, 2021
Published: January 24, 2022

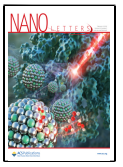

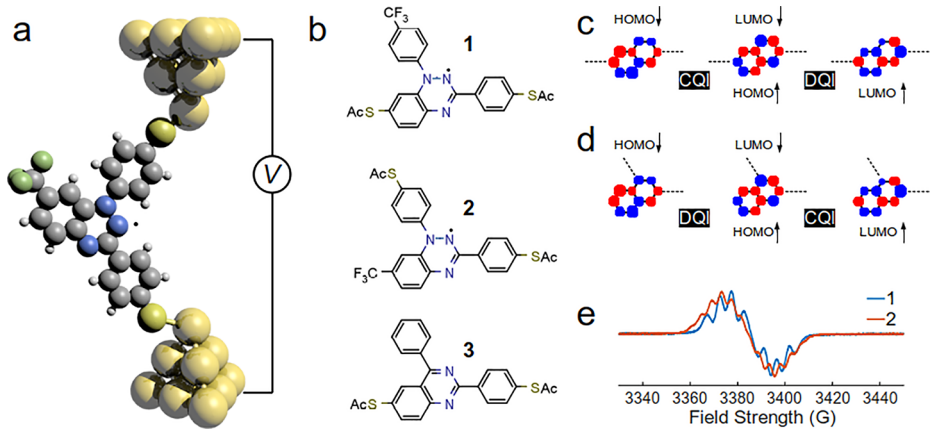

Figure 1. Molecular structure of the junctions. (a) Schematic diagram of a single-molecule junction formed by molecule **2** between gold electrodes. (b) Blatter radicals **1** and **2** with *para* and *meta* connection points and non-radical analogue **3**, tight-binding (TB) spin-up (↑) and spin-down (↓) molecular orbitals for Blatter radical core with *para* (c) and *meta* (d) connectivities. (e) EPR spectra for radicals **1** and **2**.

pseudo-*meta* (*meta*) and pseudo-*para* (*para*) connections to two gold electrodes (Figure 1a,b). Our orbital analysis[18,20] of the molecular core (see the Supporting Information for detail) indicates that destructive quantum interference (DQI) of electrons with majority spin (spin-up) is expected for *para*-connected radical molecule **1** but constructive QI (CQI) for *meta*-connected radical molecule **2**. This is in contrast to what is normally expected for the *meta*-connected conjugated polyaromatic hydrocarbons, e.g., DQI in *meta*-OPE3.[21,22] From the orbital structure of the Blatter radical core, it is clear that the highest occupied molecular orbital (HOMO) for spin-up electrons is similar to the lowest unoccupied molecular orbital (LUMO) of spin-down electrons (Figure 1c,d and Figure S1 in the Supporting Information). Also, the LUMO orbital for spin-up electrons is similar to LUMO+1 of spin-down electrons. From the simple orbital rule (eq 1 in the Supporting Information), it is clear that QI is destructive for spin-down but constructive for spin-up. Therefore, CQI (DQI) is expected for spin-down (-up) electrons in the *meta*-connected Blatter radical (Figure 1c), whereas DQI (CQI) is expected for spin-down (-up) electrons in the *para*-connected Blatter radical (Figure 1d), which is also confirmed by our quantum transport calculations below. This counterintuitive behavior is due to the localization of the spin density on nitrogen atoms in Blatter radicals (see section I.1 of the Supporting Information for a detailed discussion).

Figure 1a shows a schematic diagram of the junctions formed by a molecule with a Blatter radical core contacted to the electrodes through *meta* connectivity. To test our hypothesis that radical molecules should enhance S and G, we first studied theoretically the transport properties of the junctions formed by molecules **1**−**3** between gold electrodes using first principle computations. For this purpose, the material-specific mean-field Hamiltonians were obtained from the optimized geometry of the junctions using density functional theory (DFT).[23] The resulting Hamiltonians were then combined with the quantum transport code GOLLUM[18,24] to calculate the transmission coefficient $T(E)$ for electrons passing from the hot electrode to the cold electrode through Blatter radical cores. $T(E)$ is combined with the Landauer formula[18] to obtain the electrical conductance (see the Computational Methods).

Since Blatter radicals are spin polarized, the total transmission coefficient $T = (T^{\uparrow} + T^{\downarrow})/2$ was computed from the transmission coefficients of majority (↑) and minority (↓) spins. Figure 2a shows the total transmission coefficient $T(E)$ for electrons with energy E traversing molecules **1**−**3**. Blue and yellow curves in Figure 2a show T for *para*-connected compounds **1** and **3**, whereas the red curve shows the transmission T for *meta*-connected radical **2**. The transmission through the *meta*-connected **2** is surprisingly higher than that through the *para*-connected radical **1**. As discussed in the Supporting Information, this is because the transport due to the majority spins (blue curves in Figure S3 of the Supporting Information) is governed by a destructive QI feature in the *para*-connected molecule **1**, compared to constructive QI in the *meta*-connected molecule **2**. The spin density localized on nitrogen atoms (Figure 2d) is responsible for this counterintuitive behavior (see the Supporting Information for details).

In radical molecules **1** and **2**, two new resonances are formed within the HOMO−LUMO gap of the closed-shell analogue **3**. These new resonances close to the Fermi energy are predicted to increase the electrical conductance of the junctions. Our calculations show that this is indeed the case and radical molecules **1** and **2** show higher electrical conductance compared to the non-radical analogue **3** close to resonance around $E = -0.5$ eV (Figure 2a). However, around the DFT Fermi energy ($E = 0$ eV in Figure 2a), the predicted conductance order is **2** > **3** > **1** which is due to the effect of QI taking place in the co-tunnelling regime. Molecule **3** is a non-radical connected to electrodes through *para* connectivity, and CQI is expected. However, in its radical counterpart (molecule **1**), destructive QI of majority spins is obtained (see section I2 of the Supporting Information), which lowers the conductance. The crucial point is that, in the junctions with CQI features (molecules **2** and **3**), the radical is predicted to show high G (Figure 2b). Due to the new resonance transport through majority spins close to E_F, the room temperature S (Figure 2c) is also enhanced in radicals.

To confirm our predictions, the radical and closed-shell molecules in Figure 1 were synthesized and their single-molecule conductance and Seebeck coefficients were measured. Using a modified Naugebauer's approach[25,26] of Pd/DBU cyclization of diarylylbenzimidohydrazide derivatives, new diiodo-Blatter radicals were targeted with isomeric *para* and *meta* anchoring thioacetyl groups and with electron withdrawing substituent CF_3 (see Scheme 1 in the Supporting Information), to tune the system's electronic properties. The

https://doi.org/10.1021/acs.nanolett.1c03698
Nano Lett. 2022, 22, 948−953

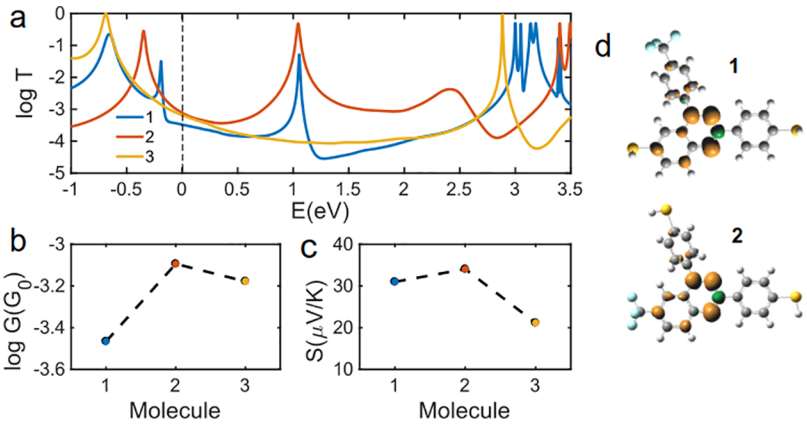

Figure 2. Quantum transport through radical molecules. (a) Total transmission coefficient $T(E) = T^{\uparrow}(E)/2 + T^{\downarrow}(E)/2$, where ↑ and ↓ denote spin up and spin down, respectively (see the Supporting Information for $T^{\uparrow}(E)$ and $T^{\downarrow}(E)$). (b) Room temperature electrical conductance at DFT Fermi energy (dashed line in part a). (c) Room temperature Seebeck coefficient at the DFT Fermi energy (dashed line in part a). (d) Spin density for radical molecules **1** and **2**.

isolated diiodo-Blatter radicals were functionalized with thioacetate by Soria-Castro's approach,[27] using potassium thioacetate under catalytic conditions, to substitute the iodo groups with thioacetates to yield **1** and **2** as pure compounds, as characterized by high resolution mass spectrometry (HR-MS), elemental analysis, EPR, and UV−visible spectroscopy. The electron withdrawing substituent (CF_3) improved the stability of the radicals. This feature was designed to prevent oxidation of radicals in the junctions.[19] Although the thioacetate coupling reaction with the hydrogen and methoxy substituted analogues produced detectable quantities of the desired products, they could not be isolated as pure compounds due to decomposition during chromatography (see the Supporting Information). It is proposed that the addition of the electron withdrawing group localizes the unpaired electron (compared to H and OMe) reducing the potential to facilitate decomposition processes.

To provide a closed-shell analogue to the Blatter radicals, 6-iodo-2-(4-iodophenyl)-4-phenylquinazoline (prepared by Lv's method)[28] was also coupled with thioacetate. Electron paramagnetic resonance (EPR) measurements (Figure 1e) confirm the radical nature of **1** and **2**. Samples for EPR measurements at room temperature were prepared by solvating the Blatter radicals in dichloromethane (DCM) with a final concentration of radicals of ca. 0.5 mM. Comparisons between experimental and simulated EPR spectra of radical molecules **1** and **2** are shown in Figures S30−32. Magnetic parameters obtained from the fitting of EPR spectra and the estimated spin densities on the nitrogen atoms in the benzotriazinyl ring and, where applicable, on the carbon atom of CF_3 are given in Tables S1 and S2 of the Supporting Information, respectively. The results indicate that the spin density in both radicals is predominantly localized on the *N* atoms in the benzotriazinyl ring (ca. 75%) in agreement with our spin density calculations (Figure 2d).

The conductance and Seebeck coefficient measurements of the three molecules were performed using a home-built scanning tunnelling microscope (STM) and the STM break-junction technique (STM-BJ)[29] at room temperature and under ambient conditions. Conductance histograms were built from thousands of current−displacement (*IZ*) traces, acquired by indenting the tip into the sample and retracting it subsequently. *IZ* curves showing features of molecular junction formation (i.e., molecule-characteristic conductance plateaus) were identified and separated from the rest by means of a nonsupervised clustering technique (*k*-means[30−32]). The clustering technique was also applied to the selected *IZ* traces to find different conductance behaviors for each compound, resulting in three different conductance clusters in all cases (Figures S33 and S34 in the Supporting Information).

For each molecule, the three clusters identified have been named as *high-plateau* (HP), *middle-plateau* (MP), and *low-plateau* (LP) clusters and each of them corresponds to a different, statistically significant junction configuration. We attribute LP to formation of $\pi-\pi$ stacked molecular junctions[19] and HP to molecular conformations with more than one connected point to each electrode. A complete discussion on these configurations can be found in the Supporting Information, and for the goal of the present work, we now focus on the *middle-plateau* (MP) clusters. These correspond to single-molecule junctions with the electrodes connected to the molecules through the anchor groups, in an equivalent way to the junctions considered in the theoretical calculations (Figure 1a). Parts a−c of Figure 3 show the 1D conductance histograms for this cluster of the three investigated compounds. Each conductance peak is fitted with a Gaussian distribution, with the mean value G_m being the most probable conductance value of the corresponding compound. The values measured (Figure 3d) show that the *meta*-connected radical **2** presents the highest conductance ($G_{m,2} = 10^{-3.5}G_0$), while the *para*-connected radical **1** shows the lowest conductance ($G_{m,1} = 10^{-4}G_0$) in this series, in good agreement with our theoretical predictions (Figure 2b).

To measure the Seebeck coefficient of the molecular junctions, a temperature difference (ΔT) is applied between the tip and the sample and the resulting thermovoltage (V_{th}) through the junction is measured. In our STM, this temperature difference is established by heating up the tip with a 1 KΩ surface resistor placed into the tip holder, while keeping the substrate at room temperature. To measure the thermovoltage of the junctions, small current−voltage (*IV*) curves were performed while the molecular junction was formed, momentarily stopping the tip displacement and ramping the voltage between ±10 mV. From these curves, V_{th} and *G* are simultaneously obtained from its zero-current crossing point and its slope, respectively (see details in the

https://doi.org/10.1021/acs.nanolett.1c03698
Nano Lett. 2022, 22, 948−953

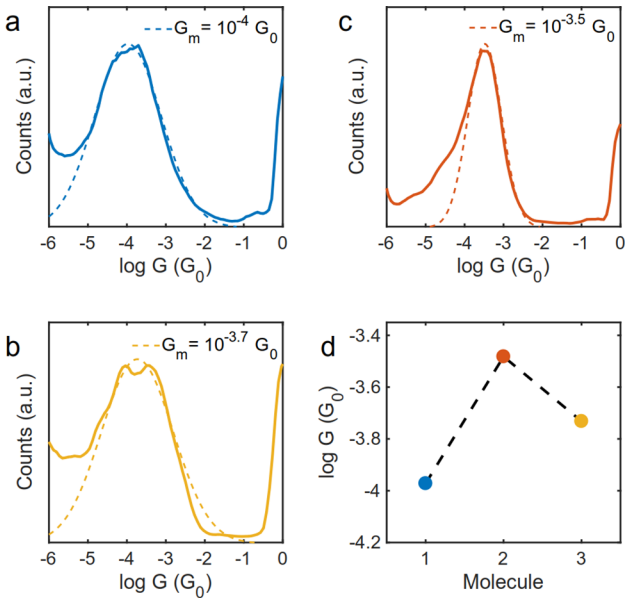

Figure 3. Experimental 1D conductance histograms for single-molecule junctions. (a–c) 1D conductance histograms for compounds **1**, **2**, and **3**, respectively (same colors as in Figure 2a). Only the data points corresponding to the *middle-plateau* (MP) cluster, identified and separated with a clustering technique, are included. Each molecular peak is fitted with a Gaussian distribution (dashed line), and its mean value G_m is given in the corresponding panel. (d) Most probable conductance value for each compound investigated, G_m, obtained from the mean value of each Gaussian fit shown in parts a–c.

Supporting Information). For consistency with the electrical conductance characterization and the previously described clustering technique, thermovoltage values corresponding to *IZ* curves in the MP clusters (single-molecule junctions) are used for the analysis. Additionally, several experimental runs were performed for each ΔT applied, which in the experiments varies between 0 and 30 K. A Gaussian distribution fitted to each experimental run gives the mean thermovoltage value ($\overline{V_{th}}$) and the standard deviation (σ_{th}) of each measurement, plotted in Figures 4a–c as empty circles and error bars, respectively. Since the Seebeck coefficient is given by $S = -V_{th}/\Delta T$, it can be directly obtained from the slope of a linear regression applied to all of the V_{th} vs ΔT data points (Figure 4a–c). In particular, the S of radical **2** (25.9 μV/K) is approximately a factor of 3 higher than that of the closed-shell compound **3** (8.4 μV/K). Indeed, the value for the *para*-connected radical **2** is, to date, one of the highest reported experimental Seebeck coefficients for a single molecule at room temperature.[3] Simultaneous enhancement of S and G in radical **2** leads to more than one order of magnitude increase of the power factor ($P = S^2G$) in **2** compared to the closed-shell molecule **3** ($P_2/P_3 = (25.9\mu/8.4\mu)^2 \times (10^{-3.5}G_0)/(10^{-3.7}G_0) = 15.1$). Furthermore, the positive sign of S for the three molecules investigated is an indication of HOMO-dominated transport in all cases.

For direct comparison of the three compounds, Figures 3d and 4d collect the experimental G_m and S values of each molecule. The enhancement of both magnitudes (G and S) for radical **2** is in good agreement with our theoretical results (Figure 2b,c and Figure S4). Furthermore, in order to demonstrate that the electron withdrawing CF_3 group increases the stability of the radicals, we have also studied an analogue of molecule **1** with a stronger electron withdrawing group (NO_2), as shown in Figure S39 of the Supporting Information. The EPR spectrum of this compound (**1a**) confirms its radical nature (Figure S31). The electron withdrawing group moves the energy levels (e.g., HOMO and LUMO) down in energy and thereby stabilizes the molecule further. This comes with the cost of moving the singly occupied energy level away from the Fermi energy. Consequently, G and S are expected to decrease compared to the CF_3 analogue (molecule **1**). This is confirmed by our calculated and measured G and S (see Figures S3 and S39).

To experimentally reinforce the evidence of resonances close to the Fermi energy, we also explored the transmission curve by means of spectroscopy experiments performed for all compounds. Large current–voltage curves (±1 V) were

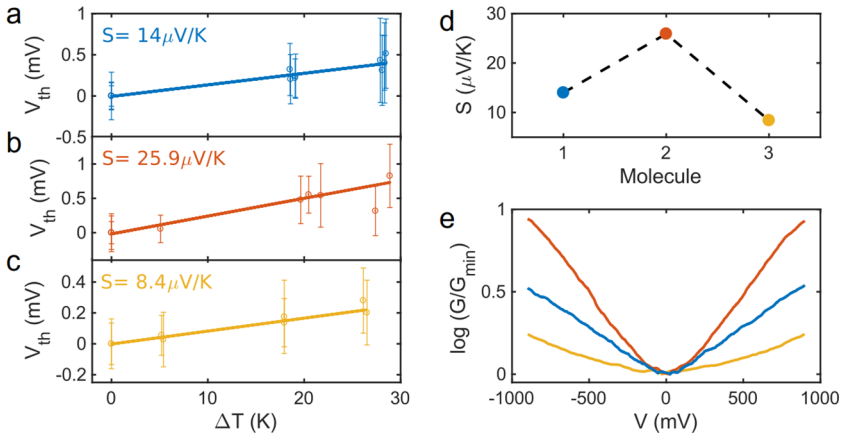

Figure 4. Experimental Seebeck coefficient S for single-molecule junctions. (a–c) Mean thermovoltage ($\overline{V_{th}}$) and standard deviation values (σ_{th}) from Gaussian fits applied to each experimental run performed, i.e., to the individual thermovoltage (V_{th}) values measured for each temperature difference (ΔT). $\overline{V_{th}}$ and σ_{th} are represented by empty circles and error bars, respectively. The Seebeck coefficient of each compound **1**–**3** (a–c) is the slope of a linear regression to all of the individual V_{th} vs ΔT data points, and the values obtained are given in the corresponding panel (same colors as in Figure 2a). (d) Seebeck coefficient of the three compounds investigated. The values are obtained from the slope of the linear regressions shown in parts a–c. (e) Average conductance–voltage (GV) of all current–voltage curves taken in the molecular junctions, normalized by the G value at low bias voltage (G_{min}) for each compound (see the Supporting Information and Figure S37).

https://doi.org/10.1021/acs.nanolett.1c03698
Nano Lett. 2022, 22, 948–953

measured, while forming the molecular junctions, and were plotted as conductance−voltage (GV) curves, where $G = I/V$ (see more details in the Supporting Information). Considering only the junctions with a clear molecular plateau, 2D histograms of all GV curves with a low-V_{bias} conductance between $10^{-4}G_0$ and $10^{-5}G_0$, as well as their average traces, are shown in Figure S37. For direct comparison of the shape of the GV curves, the normalized average traces for each compound are shown in Figure 4e. The GV curves of compound **3** are flatter than those of compounds **1** and **2**, which are more "V"-shaped, especially in the case of molecule **2**, which supports the presence of a resonance closer to the Fermi energy of the electrodes in radical compounds, in contrast to the closed-shell quinazoline analogue.

In summary, using a combined experimental and theoretical study, we demonstrated that both the Seebeck coefficient and the electrical conductance can be enhanced in Blatter radicals, compared to a closed-shell analogue, leading to a more than one order of magnitude enhancement of the power factor in the radical molecule. This enhancement should be a generic feature of radicals which create resonances close to the Fermi energy of the electrodes. This leads to the observation of a high value of S for an organic molecule in a single-molecular junction. This ground-breaking strategy is potentially a versatile design route that exploits unpaired spins of neutral or charged species for creating room temperature single-molecule thermoelectric junctions and ultrathin film thermoelectric materials for efficient conversion of waste heat to electricity or for on-chip cooling of CMOS-based technology in consumer electronic devices.

METHODS

Computational Methods. The optimized geometries with ground-state Hamiltonian and overlap matrix elements for gas phase molecules and molecules between electrodes were obtained using DFT. These results were then combined with the Green function method to calculate the phase-coherent, elastic-scattering properties of the system, consisting of two gold electrodes and the molecule as the scattering region. From the calculated transmission functions for majority and minority spins, the electrical conductance and Seebeck coefficient were calculated. See the Supporting Information for details of computational methods.

Molecular Synthesis. The Supporting Information contains experimental procedures and NMR spectra.

Experimental Methods. Conductance, Seebeck coefficient, and spectroscopy measurements were carried out using a home-built STM at room temperature and under ambient conditions. Samples were prepared using the drop-casting technique by immersing the previously annealed Au(111) samples in a 1 mM DCM solution of the target compound for 40 min and then allowing them to dry. Mechanically cut Au wires (0.25 mm diameter, 99.99% purity, Goodfellow) were used as STM tips. Analysis of the data was done using MATLAB, and a clustering technique was implemented using the k-means function. More information about the experimental methods is in the Supporting Information.

ASSOCIATED CONTENT

Supporting Information

The Supporting Information is available free of charge at https://pubs.acs.org/doi/10.1021/acs.nanolett.1c03698.

Details of the calculations, synthesis and measurement methods and supporting results including DFT and tight-binding orbitals for molecules, additional transmission coefficient calculations, synthetic routes and characterizations, NMR and EPR data, and STM measurements (PDF)

AUTHOR INFORMATION

Corresponding Authors

Ross Davidson − *Department of Chemistry, Durham University, Durham DH1 3LE, United Kingdom*; Email: ross.davidson@durham.ac.uk

Martin R. Bryce − *Department of Chemistry, Durham University, Durham DH1 3LE, United Kingdom*; orcid.org/0000-0003-2097-7823; Email: m.r.bryce@durham.ac.uk

Nicolás Agraït − *Departamento de Física de la Materia Condensada, Universidad Autónoma de Madrid, E-28049 Madrid, Spain; Condensed Matter Physics Center (IFIMAC) and Instituto Universitatio de Ciencia de Materiales "Nicolás Cabrera" (INC), Universidad Autónoma de Madrid, E-28049 Madrid, Spain; Instituto Madrileño de Estudios Avanzados en Nanociencia IMDEA-Nanociencia, E-28049 Madrid, Spain*; orcid.org/0000-0003-4840-5851; Email: nicolas.agrait@uam.es

Hatef Sadeghi − *Device Modelling Group, School of Engineering, University of Warwick, CV4 7AL Coventry, United Kingdom*; orcid.org/0000-0001-5398-8620; Email: Hatef.Sadeghi@warwick.ac.uk

Authors

Juan Hurtado-Gallego − *Departamento de Física de la Materia Condensada, Universidad Autónoma de Madrid, E-28049 Madrid, Spain*

Sara Sangtarash − *Device Modelling Group, School of Engineering, University of Warwick, CV4 7AL Coventry, United Kingdom*

Laura Rincón-García − *Departamento de Física de la Materia Condensada, Universidad Autónoma de Madrid, E-28049 Madrid, Spain*; orcid.org/0000-0002-2408-0928

Abdalghani Daaoub − *Device Modelling Group, School of Engineering, University of Warwick, CV4 7AL Coventry, United Kingdom*

Gabino Rubio-Bollinger − *Departamento de Física de la Materia Condensada, Universidad Autónoma de Madrid, E-28049 Madrid, Spain; Condensed Matter Physics Center (IFIMAC) and Instituto Universitatio de Ciencia de Materiales "Nicolás Cabrera" (INC), Universidad Autónoma de Madrid, E-28049 Madrid, Spain*; orcid.org/0000-0001-7864-8980

Colin J. Lambert − *Physics Department, Lancaster University, Lancaster LA1 4YB, United Kingdom*; orcid.org/0000-0003-2332-9610

Vasily S. Oganesyan − *School of Chemistry, University of East Anglia, Norwich NR4 7TJ, United Kingdom*

Complete contact information is available at: https://pubs.acs.org/10.1021/acs.nanolett.1c03698

Author Contributions

○J.H.-G., S.S., R.D.: These authors contributed equally.

Notes

The authors declare no competing financial interest.

https://doi.org/10.1021/acs.nanolett.1c03698
Nano Lett. 2022, 22, 948−953

All information to reproduce simulation data is provided in the manuscript. The underlying experimental and simulation data can be accessed by contacting the corresponding authors.

■ ACKNOWLEDGMENTS

H.S. acknowledges the UKRI for Future Leaders Fellowship number MR/S015329/2. S.S. acknowledges the Leverhulme Trust for Early Career Fellowship no. ECF-2018-375. J.H.-G., R.D., L.R.-G., C.J.L, M.R.B., and N.A. acknowledge funding from EC H2020 FET Open project grant agreement number 767187 "QuIET". M.R.B. thanks EPSRC grant EP/K0394/23/1 and EC H2020 FET Open project grant agreement number 766853 "EFINED" for funding. N.A. and L.R.-G. acknowledge funding from the Education and Research Council of the Comunidad de Madrid and the European Social Fund (ref. PEJD-2019-POST/IND-16353). N.A. and G.R.-B. acknowledge funding from the Comunidad de Madrid NANOMAGCOST-CM (P2018/NMT-4321) and from the Spanish Ministry of Science and Innovation, through grants MAT2017-88693-R and the "María de Maeztu" Programme for Units of Excellence in R&D (CEX2018-000805-M). V.S.O. acknowledges support from EPRSC (Grant EP/P007554/1).

■ REFERENCES

(1) Russ, B.; Glaudell, A.; Urban, J. J.; Chabinyc, M. L.; Segalman, R. A. Organic Thermoelectric Materials for Energy Harvesting and Temperature Control. *Nat. Rev. Mater.* **2016**, *1* (10), 16050.
(2) Wang, K.; Meyhofer, E.; Reddy, P. Thermal and Thermoelectric Properties of Molecular Junctions. *Adv. Funct. Mater.* **2020**, *30* (8), 1904534.
(3) Rincón-García, L.; Evangeli, C.; Rubio-Bollinger, G.; Agraït, N. Thermopower Measurements in Molecular Junctions. *Chem. Soc. Rev.* **2016**, *45* (15), 4285−4306.
(4) Cui, L.; Jeong, W.; Fernández-Hurtado, V.; Feist, J.; García-Vidal, F. J.; Cuevas, J. C.; Meyhofer, E.; Reddy, P. Study of Radiative Heat Transfer in Ångström- and Nanometre-Sized Gaps. *Nat. Commun.* **2017**, *8*, 14479.
(5) Lee, S.; Kim, S.; Pathak, A.; Tripathi, A.; Qiao, T.; Lee, Y.; Lee, H.; Woo, H. Y. Recent Progress in Organic Thermoelectric Materials and Devices. *Macromol. Res.* **2020**, *28* (6), 531−552.
(6) Sadeghi, H.; Sangtarash, S.; Lambert, C. J. Oligoyne Molecular Junctions for Efficient Room Temperature Thermoelectric Power Generation. *Nano Lett.* **2015**, *15* (11), 7467−7472.
(7) Hinterleitner, B.; Knapp, I.; Poneder, M.; Shi, Y.; Müller, H.; Eguchi, G.; Eisenmenger-Sittner, C.; Stöger-Pollach, M.; Kakefuda, Y.; Kawamoto, N.; Guo, Q.; Baba, T.; Mori, T.; Ullah, S.; Chen, X.-Q.; Bauer, E. Thermoelectric Performance of a Metastable Thin-Film Heusler Alloy. *Nature* **2019**, *576* (7785), 85−90.
(8) Zhao, L.-D.; Lo, S.-H.; Zhang, Y.; Sun, H.; Tan, G.; Uher, C.; Wolverton, C.; Dravid, V. P.; Kanatzidis, M. G. Ultralow Thermal Conductivity and High Thermoelectric Figure of Merit in SnSe Crystals. *Nature* **2014**, *508* (7496), 373−377.
(9) Zhao, L.-D.; Dravid, V. P.; Kanatzidis, M. G. The Panoscopic Approach to High Performance Thermoelectrics. *Energy Environ. Sci.* **2014**, *7* (1), 251−268.
(10) Martin, L. W.; Rappe, A. M. Thin-Film Ferroelectric Materials and Their Applications. *Nat. Rev. Mater.* **2017**, *2* (2), 16087.
(11) Wei, J.; Yang, L.; Ma, Z.; Song, P.; Zhang, M.; Ma, J.; Yang, F.; Wang, X. Review of Current High-ZT Thermoelectric Materials. *J. Mater. Sci.* **2020**, *55* (27), 12642−12704.
(12) Tsutsui, M.; Morikawa, T.; He, Y.; Arima, A.; Taniguchi, M. High Thermopower of Mechanically Stretched Single-Molecule Junctions. *Sci. Rep.* **2015**, *5* (1), 11519.
(13) Al-Galiby, Q. H.; Sadeghi, H.; Algharagholy, L. A.; Grace, I.; Lambert, C. Tuning the Thermoelectric Properties of Metallo-Porphyrins. *Nanoscale* **2016**, *8* (4), 2428−2433.
(14) Fan, Z.; Ouyang, J. Thermoelectric Properties of PEDOT:PSS. *Adv. Electron. Mater.* **2019**, *5* (11), 1800769.
(15) Gayner, C.; Kar, K. K. Recent Advances in Thermoelectric Materials. *Prog. Mater. Sci.* **2016**, *83*, 330−382.
(16) Wang, H.; Yu, C. Organic Thermoelectrics: Materials Preparation, Performance Optimization, and Device Integration. *Joule* **2019**, *3* (1), 53−80.
(17) Sangtarash, S.; Sadeghi, H. Radical Enhancement of Molecular Thermoelectric Efficiency. *Nanoscale Adv.* **2020**, *2* (3), 1031−1035.
(18) Sadeghi, H. Theory of Electron, Phonon and Spin Transport in Nanoscale Quantum Devices. *Nanotechnology* **2018**, *29* (37), 373001.
(19) Low, J. Z.; Kladnik, G.; Patera, L. L.; Sokolov, S.; Lovat, G.; Kumarasamy, E.; Repp, J.; Campos, L. M.; Cvetko, D.; Morgante, A.; Venkataraman, L. The Environment-Dependent Behavior of the Blatter Radical at the Metal−Molecule Interface. *Nano Lett.* **2019**, *19* (4), 2543−2548.
(20) Tsuji, Y.; Staykov, A.; Yoshizawa, K. Orbital Views of Molecular Conductance Perturbed by Anchor Units. *J. Am. Chem. Soc.* **2011**, *133* (15), 5955−5965.
(21) Manrique, D. Z.; Huang, C.; Baghernejad, M.; Zhao, X.; Al-Owaedi, O. A.; Sadeghi, H.; Kaliginedi, V.; Hong, W.; Gulcur, M.; Wandlowski, T.; Bryce, M. R.; Lambert, C. J. A Quantum Circuit Rule for Interference Effects in Single-Molecule Electrical Junctions. *Nat. Commun.* **2015**, *6*, 6389.
(22) Liu, X.; Sangtarash, S.; Reber, D.; Zhang, D.; Sadeghi, H.; Shi, J.; Xiao, Z. Y.; Hong, W.; Lambert, C. J.; Liu, S. X. Gating of Quantum Interference in Molecular Junctions by Heteroatom Substitution. *Angew. Chemie - Int. Ed.* **2017**, *56* (1), 173−176.
(23) Soler, J. M.; Artacho, E.; Gale, J. D.; García, A.; Junquera, J.; Ordejón, P.; Sánchez-Portal, D. The SIESTA Method for Ab Initio Order- N Materials Simulation. *J. Phys.: Condens. Matter* **2002**, *14* (11), 2745−2779.
(24) Ferrer, J.; Lambert, C. J.; García-Suárez, V. M.; Manrique, D. Z.; Visontai, D.; Oroszlany, L.; Rodríguez-Ferradás, R.; Grace, I.; Bailey, S. W. D.; Gillemot, K.; Sadeghi, H.; Algharagholy, L. A. GOLLUM: A next-Generation Simulation Tool for Electron, Thermal and Spin Transport. *New J. Phys.* **2014**, *16*, 093029.
(25) Neugebauer, F. A.; Umminger, I. Über 1,4-Dihydro-1,2,4-Benzotriazinyl-Radikale. *Chem. Ber.* **1980**, *113* (4), 1205−1225.
(26) Bodzioch, A.; Zheng, M.; Kaszyński, P.; Utecht, G. Functional Group Transformations in Derivatives of 1,4-Dihydrobenzo[1,2,4]-Triazinyl Radical. *J. Org. Chem.* **2014**, *79* (16), 7294−7310.
(27) Soria-Castro, S. M.; Peñéñory, A. B. Efficient Cu-Catalyzed Base-Free C−S Coupling under Conventional and Microwave Heating. A Simple Access to S-Heterocycles and Sulfides. *Beilstein J. Org. Chem.* **2013**, *9*, 467−475.
(28) Lv, Z.; Wang, B.; Hu, Z.; Zhou, Y.; Yu, W.; Chang, J. Synthesis of Quinazolines from N, N ′-Disubstituted Amidines via I 2 /KI-Mediated Oxidative C−C Bond Formation. *J. Org. Chem.* **2016**, *81* (20), 9924−9930.
(29) Evangeli, C.; Gillemot, K.; Leary, E.; González, M. T.; Rubio-Bollinger, G.; Lambert, C. J.; Agraït, N. Engineering the Thermopower of C_{60} Molecular Junctions. *Nano Lett.* **2013**, *13* (5), 2141−2145.
(30) Lemmer, M.; Inkpen, M. S.; Kornysheva, K.; Long, N. J.; Albrecht, T. Unsupervised Vector-Based Classification of Single-Molecule Charge Transport Data. *Nat. Commun.* **2016**, *7*, 12922.
(31) Cabosart, D.; El Abbassi, M.; Stefani, D.; Frisenda, R.; Calame, M.; van der Zant, H. S. J.; Perrin, M. L. A Reference-Free Clustering Method for the Analysis of Molecular Break-Junction Measurements. *Appl. Phys. Lett.* **2019**, *114* (14), 143102.
(32) Zotti, L. A.; Bednarz, B.; Hurtado-Gallego, J.; Cabosart, D.; Rubio-Bollinger, G.; Agrait, N.; van der Zant, H. Can One Define the Conductance of Amino Acids? *Biomolecules* **2019**, *9* (10), 580.

https://doi.org/10.1021/acs.nanolett.1c03698
Nano Lett. 2022, 22, 948−953